effects has been studied for at least 25 years (*2*). An aerosol influence on cloud albedo should show temporal and spatial variability because of the heterogeneous nature of tropospheric aerosols. But there was little interannual or seasonal variability in values of β for Cape Grim and American Samoa (Fig. 4) nor was there significant geographic variability (Fig. 3). If aerosol effects were important in determining β, these variations should be much larger. Cape Grim in particular is known to be a fairly clean site with regard to aerosols; the boundary layer concentration of cloud nuclei is largest in the period from December through February (*8*), and the aerosol optical depth at visible wavelengths peaks in the period from September through November (*9*). But values of β for these periods differ little from those obtained in March through May and June through August (Fig. 4B).

Although only two GCMs were used in this comparison between models and observations, comparable discrepancies have been reported for more detailed cloud radiative transfer models than typically used in GCMs (*1*). These studies also investigated the role of cloud interstitial water vapor and showed that this was not the cause of the enhanced absorption. The enhanced cloud SW absorption phenomenon is of significant magnitude. Averaged over the globe and annually, $C_s(\mathrm{TOA}) \approx -50\ \mathrm{W\ m^{-2}}$ (*10*), whereas the average observed value for β is 0.55 versus 0.80 for the GCMs (Fig. 3). For a global mean surface albedo of 0.1, Eq. 2 indicates that enhanced cloud SW absorption, by itself, should reduce global mean SW surface absorption by about 25 $\mathrm{W\ m^{-2}}$ relative to contemporary climate models. This significant discrepancy is consistent with a comparison of four GCMs to surface measurements (*11*) in which cloud effects were not isolated and the TOA SW flux was not constrained. Our finding of enhanced cloud SW absorption is also consistent with an earlier satellite-surface measurement study restricted to the eastern United States (*12*).

REFERENCES AND NOTES

1. V. Ramanathan *et al.*, *Science* **267**, 499 (1995).
2. G. L. Stephens and S.-C. Tsay, *Q. J. R. Meteorol. Soc.* **116**, 671 (1990); I. N. Mel'nikova and V. V. Mikhaylov, *J. Atmos. Sci.* **51**, 925 (1994).
3. R. D. Cess *et al.*, *J. Climate* **6**, 308 (1993).
4. For the BAO tower, average TOA reflectances were computed for 12 by 12 arrays of half-hourly GOES-West 1-km pixels as described (*13*) and converted to narrow-band albedos with the use of the ERBE anisotropic reflectance model (*14*), which varies with the degree of cloudiness. The same technique was applied to 8 by 8 arrays of hourly GOES-East 1-km pixels over each of the Wisconsin pyranometer locations (*15*) with the use of the conversion from brightness counts to reflectance (*16*). Narrow-band albedos were then converted to broad-band albedos for both locations (*17*).
5. The data were taken at sites where extensive attention was given to ongoing calibration and operational accuracy. Also, calibration errors and residual long-term drifts were eliminated through the regression analyses, as was also the case for the satellite measurements.
6. S. Nemesure *et al.*, *J. Climate* **7**, 579 (1994).
7. K. E. Trenberth, *NCAR TN-73+STR* (National Center for Atmospheric Research, Boulder, CO, 1992).
8. J. L. Gras, *J. Atmos. Chem.* **11**, 89 (1989).
9. B. W. Forgan and P. J. Fraser, *Baseline Atmospheric Program (Australia) 1985* (Australian Bureau of Meteorology, Melbourne, 1987).
10. E. F. Harrison *et al.*, *J. Geophys. Res.* **95**, 18687 (1990).
11. J. R. Garratt, *J. Climate* **7**, 72 (1994).
12. C. G. Justus, *Proceedings of the Conference on Satellite Meteorology/Remote Sensing Applications* (American Meteorological Society, Boston, MA, 1984), p. 197.
13. P. Minnis *et al.*, *J. Appl. Meteorol.* **31**, 317 (1992).
14. J. T. Suttles *et al.*, "Angular radiation models for Earth-atmosphere system," *NASA RP-1184* (1988), shortwave radiation, vol. 1.
15. C. H. Whitlock *et al.*, *NASA TM 100485* (1987); C. H. Whitlock *et al.*, *NASA TM 102596* (1990). Of the 17 pyranometers, we used only those 11 that provided continuous measurements throughout the measurement period, which started at noon LT on 12 October 1986 and extended through 2 November 1986.
16. P. Minnis, P. W. Heck, D. F. Young, *J. Atmos. Sci.* **50**, 1305 (1993).
17. The broad-band albedo (α_B) was estimated from the narrow-band albedo (α_N) through

$$\alpha_B = a_0 + a_1\alpha_N + a_2\alpha_N^2 + a_3 \ln(\sec\theta_0)$$

where θ_0 is the solar zenith angle. For the BAO tower location, the coefficients a_i were determined through multiple regression with the use of 2.5° by 2.5° ERBS and NOAA 9 ERBE-scanner instantaneous albedos and matched to 2.5° by 2.5° GOES narrow-band albedos. To ensure that background and atmospheric conditions were similar to those in the vicinity of the BAO tower, we took regression data between 100°W and 105°W and 35°N to 45°N, during the same period as the Boulder GOES-data. A similar procedure, using ERBS, was applied to the Wisconsin sites, with the regression coefficients based on 2.5° by 2.5° data between 90°W and 100°W and 35°N to 45°N, during October 1986.

18. This research was supported by Department of Energy (DOE) grants DEFG0285ER60314 and DEFG0290ER61063 and NASA grants NAG11264 and NAGW3517 to the State University of New York at Stony Brook; by DOE grant DEFG0593ER61376 to the National Center for Atmospheric Research, which is sponsored by NSF; by the NOAA Climate Monitoring and Diagnostics Laboratory; by NSF grants ATM 8920119 and ATM 9011259 to the Scripps Institution of Oceanography; and by DOE contract W-7405-ENG-48 to Lawrence Livermore National Laboratory. The ECMWF's permission to use their GCM in this study is gratefully acknowledged.

24 August 1994; accepted 14 November 1994

Warm Pool Heat Budget and Shortwave Cloud Forcing: A Missing Physics?

V. Ramanathan,* B. Subasilar, G. J. Zhang, W. Conant, R. D. Cess, J. T. Kiehl, H. Grassl, L. Shi

Ship observations and ocean models indicate that heat export from the mixed layer of the western Pacific warm pool is small (<20 watts per square meter). This value was used to deduce the effect of clouds on the net solar radiation at the sea surface. The inferred magnitude of this shortwave cloud forcing was large (≈−100 watts per square meter) and exceeded its observed value at the top of the atmosphere by a factor of about 1.5. This result implies that clouds (at least over the warm pool) reduce net solar radiation at the sea surface not only by reflecting a significant amount back to space, but also by trapping a large amount in the cloudy atmosphere, an inference that is at variance with most model results. The excess cloud absorption, if confirmed, has many climatic implications, including a significant reduction in the required tropics to extratropics heat transport in the oceans.

What effect do clouds have on the atmospheric solar absorption? This question is fundamental to the issue of how clouds influence climate and climate change. Clouds reduce the solar radiation absorbed by the surface-atmosphere system—that is, the shortwave (SW) cloud forcing at the top of the atmosphere [$C_s(\mathrm{TOA})$] is less than 0. The global annual mean value for $C_s(\mathrm{TOA})$ (*1*) is about −45 to −50 $\mathrm{W\ m^{-2}}$. This value is negative because clouds in general reflect more solar radiation back to space than a cloudless atmosphere. $C_s(\mathrm{TOA})$ can be partitioned in terms of $C_s(\mathrm{S})$, the effect of clouds on the surface, and of $C_s(\mathrm{A})$, the effect on the atmospheric column. If clouds enhance the solar absorption by the atmospheric column when compared to the solar absorption with a clear-sky atmosphere, then $C_s(\mathrm{A}) > 0$. Here, we used measurements of oceanic heat transport and of the surface heat budget in the warm western Pacific ocean to deduce values for $C_s(\mathrm{A})$. A companion

V. Ramanathan, B. Subasilar, G. J. Zhang, W. Conant, Center for Clouds, Chemistry and Climate, Scripps Institution of Oceanography, University of California at San Diego, La Jolla, CA 92093, USA.
R. D. Cess, Institute for Terrestrial and Planetary Atmospheres, Marine Science Research Center, State University of New York, Stony Brook, NY 11794, USA.
J. T. Kiehl, National Center for Atmospheric Research, Boulder, CO 80307, USA.
H. Grassl, Max-Planck-Institut Fur Meteorologie, Bundesstraße 55, D-020146 Hamburg, Germany.
L. Shi, SeaSpace Corporation, San Diego, CA 92126, USA.

*To whom correspondence should be addressed.

study (2) obtains $C_s(A)$ from radiometric measurements at TOA and at the surface.

The warm pool (WP) extends roughly between 140°E to 170°E and 10°N to 10°S. Annual mean sea-surface temperature (SST) in this region attains the maximum value (≈302.5 K) observed for oceans. The WP atmosphere is humid and cloudy; the frequency of deep convection reaches about 60% (3). WP SSTs have been remarkably stable on geological time scales (4), and the WP may play a role in the El Niño Southern Oscillation (5). Two major field experiments, TOGA-COARE and CEPEX (6), were recently conducted to quantify the processes that govern the WP and equatorial Pacific heat budget.

An intriguing feature of the WP (7, 8) is that the annual mean dynamical heat transport (D) out of the WP mixed layer by both the horizontal advection and the vertical diffusion is small. Specifically, recent studies suggested that $0 \leq D \leq 20$ W m^{-2}. This, in turn, constrains the long-term annual mean net downward surface heat flux (H) to small values, because there should be no net heating, ($H - D$), of the mixed layer over an annual cycle (9). Here, we used this condition to try to close the heat budget of the WP with use of available data. We deduce that a large reduction (≈100 W m^{-2}) of surface insolation by clouds is needed; this in turn requires that $C_s(A)$ is large (≈35 W m^{-2}) over the WP. A companion study (2) supports this inference and concludes that the anomalous solar absorption may be a feature of other cloudy regions of the planet as well.

The net heat flux, H, at the sea surface can be expressed as

$$H = S_a + C_s(S) - F - E - h \quad (1)$$

We separated the absorbed solar radiation at the surface into two terms: S_a, the net (down minus up) solar radiation under clear skies and $C_s(S)$. F is the net (up minus down) longwave (LW) radiation, E is the evaporative heat flux, and h is the turbulent sensible heat flux. The net heating of the mixed layer is

$$Q = H - D \quad (2)$$

D is a sum of two terms: D_a, the horizontal advection of heat from the mixed layer into the surrounding oceans, and D_e, the downward entrainment of heat into the thermocline below.

Unless otherwise explicitly stated, all of the quantities represent an average for the region between 140°E to 170°E and 10°N to 10°S. To obtain estimates of these terms, we analyzed recent data (10) from COADS, ERBE, TOGA-TAO moorings, CEPEX, and several pre-TOGA research vessel cruises (8). The one exception is $C_s(S)$: Lack of adequate surface solar radiation observations combined with a lack of understanding of cloud-radiation interactions within cirrus clouds prevent us from estimating this quantity directly. Instead, we estimate it as a residual from Eqs. 1 and 2. Our best estimates for the terms in Eqs. 1 and 2 are shown in Fig. 1. Monthly and interannual standard deviation, 1σ, of the quantities are needed to assess the uncertainty in the long-term annual means. For values of S and F, the observational records are not of sufficient duration to estimate 1σ. We obtained monthly and interannual 1σ values from a

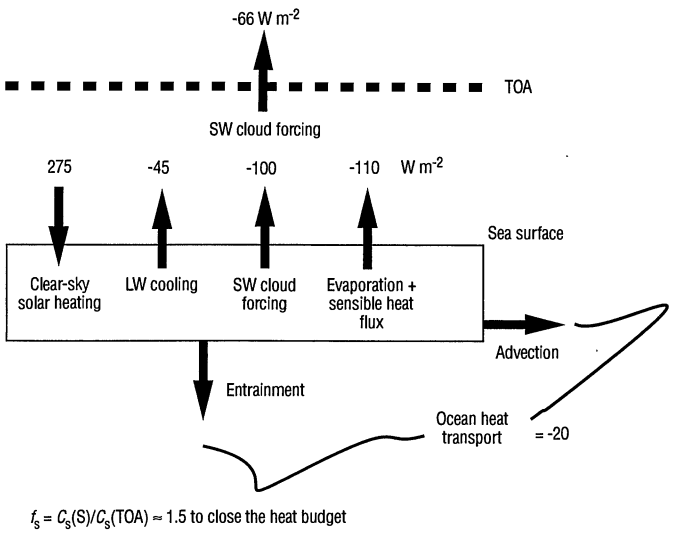

Fig. 1. Annual mean budget of the WP. Energy loss terms are shown as negative values, with outward arrows to facilitate presentation.

Table 1. Comparison of estimated clear-sky solar absorption (S_a) with in situ measurements.

S_a	Present (W m^{-2})	Surface observation (W m^{-2})	Source for surface observation
2°S and 168°E to 158°W (7 March to 16 March 1993)	302	306	CEPEX pyranometer data (*14*)
14.25°S and 170.56°W (annual mean for 1985)	268	271	Pyranometer data; American Samoa (*15*)

Table 2. Observed and estimated LW cooling at the WP sea surface. Dates and locations for the data are as follows: TOGA-COARE, 2°S and 156°E, 1 February to 28 February 1993; CEPEX, 2°S and 160°E to 170°W, 7 March to 13 March 1993; pre–TOGA-COARE, 0°N to 4°S and 150°E to 151°E, 7 May to 20 May 1988; and pre–TOGA-COARE, 0°N and 45°E, 17 February to 10 March 1990. For TOGA-COARE and CEPEX, the pyrgeometer data (*21*) were from the R/V *Vickers*, and for the first data set from pre–TOGA-COARE, the net radiometer data were from the R/V *Franklin* (*8*).

Conditions	Flux (W m^{-2})	Description
	TOGA-COARE and CEPEX	
Clear sky	59	Data for all situations without low clouds and less than 2 octas of midlevel cloud coverage
Average cloudy sky	45	All data values were used
	Pre–TOGA-COARE	
Clear sky	55	Maximum reported value was adopted
Average cloudy sky	45	All data values were used
	Pre–TOGA-COARE (0°N and 45°E)	
Average cloudy sky	39	Radiometer on board R/V *Wecoma* (*22*)
	Our study	
Clear sky	59	
Average cloudy sky	43	
	Climatology	
Average cloudy sky (annual average, WP)	40	Empirical climatological estimates (*23*)

combination of the 5-year ERBE data and a 10-year-long simulation of the WP fluxes by the National Center for Atmospheric Research three-dimensional community climate model (CCM2) (*11*).

For solar radiation, we obtained values for S_a by combining 5-year mean ERBE values for the TOA clear-sky albedo, A, with Li *et al.*'s (*12*) transfer function for converting A to net radiation at the surface in conjunction with observed WP humidity values (*13*). This method was first validated with in situ pyranometer data taken at the surface (Table 1) from a ship (R/V *Vickers*) in the central equatorial Pacific ocean (*14*) and from a meteorological station at American Samoa (*15*).

The estimated annual mean value for the WP is 275 W m^{-2}. Because we adopted a water vapor amount (≈54 kg m^{-2}) that was representative of average cloudy conditions (*13*), the estimated values for S_a do not suffer from the bias that might have resulted had we used just the data for clear-sky humidities. In summary, we adopted S_a = 275 W m^{-2} (Fig. 1) with the range 270 ≤ S_a ≤ 280 W m^{-2} (*16*).

At the surface, LW cooling (F) is equal to $\sigma T^4 - F^-$ where T is the SST and F^- is the downward emission by the atmosphere and clouds. We let $F^- = F_a^- + C_l(S)$ [where the clear sky flux is F_a^- and the LW cloud forcing at the surface is $C_l(S)$]. We calculated F_a^- using temperature and humidity soundings launched from ships from 1985 to 1989 as input to a LW radiation model (*17*). For the 5-year period, a total of 96 WP ship soundings were available. The computed clear-sky LW cooling was 59 W m^{-2}. The uncertainty attributable to sampling error (*18*) was about 1 W m^{-2}.

We computed cloudy-sky downward fluxes for various cloud types including low, middle, cumulonimbus, and cirrus clouds. Cloud distributions were obtained from satellite and ship data (*19*). The surface LW cooling was 43 W m^{-2} for the average cloudy conditions. The inclusion of clouds reduces the value from 59 to 43 W m^{-2}—that is, $C_l(S)$ = 16 W m^{-2}. To assess the magnitude of the sampling problem, we adopted another method (*20*) using the 5-year ERBE data. This method yielded a value for $C_l(S)$ of ≈19 W m^{-2}, in excellent agreement with the value of 16 W m^{-2} obtained directly from the ship sondes.

The clear-sky value for F (59 W m^{-2}) and average cloudy-sky value for F (43 W m^{-2}) are within 5 W m^{-2} of available observations and climatological estimates (*21–23*) (Table 2). It is meaningful to compare the yearly means with the ship observations because the mean monthly variation of F is estimated to be small ($1\sigma \leq 4$ W m^{-2}) (*11*). We adopted the maximum observed value of 45 W m^{-2} and a range of 35 ≤ F ≤ 45 W m^{-2} (Table 2).

Values for E and h were obtained from surface data collected continuously for about 2 years by TOGA-TAO moored buoys in the WP. These buoys measure SST, boundary layer temperature, humidity, and winds. We used these data to estimate E and h values with the bulk aerodynamic method (*24*), which accounts for the steep increase in the turbulent exchange coefficient under low wind speed; this method agrees within 10% (even under conditions of low wind speed) with the direct evaporation flux measurements taken from aircraft during CEPEX. Data from a total of 20 WP buoys were available. They were collected in the form of both daily averages and hourly averages. We have used the daily averaged data rather than the hourly data to compute E, as the latter are often not available. The sensitivity of E to different strategies of obtaining hourly data is about 1 W m^{-2}. For the three buoys for which both hourly and daily data were available (*25*), our estimate of E from the hourly data is 102 W m^{-2} and that from the daily averaged data is 89 W m^{-2} (*25*) for the data period from mid-September 1992 to late February 1993 (Fig. 2). On the basis of this comparison, we conclude that the daily data underestimates E by 13 W m^{-2}. The annual average E computed from the daily data for the 20 buoys is 88 W m^{-2}. To this, we added the bias of 13 W m^{-2} to obtain our best estimate of 100 W m^{-2} (rounded to the nearest 5 W m^{-2}), which agrees with the climatological estimate (*26*) of 100 W m^{-2}. An uncertainty of 15 W m^{-2} is assumed, which yields 85 ≤ E ≤ 115 W m^{-2}.

The annual mean value of h from the buoys is 10 W m^{-2}, which includes a 3 W m^{-2} cooling due to the colder rain drops (*27*). The range of annual mean value for h from published estimates (*23*, *24*, *26*) and the buoy data is 5 ≤ h ≤ 10 W m^{-2}. We adopted the maximum value of 10 W m^{-2}. The sum of E and h is estimated to be

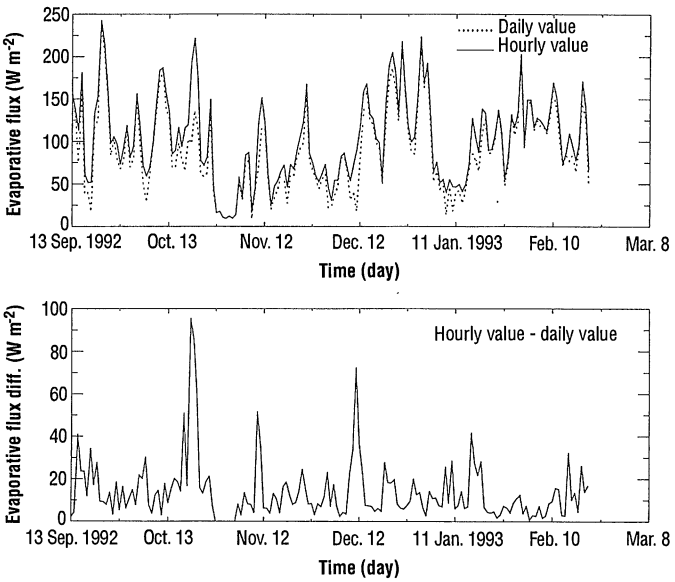

Fig. 2. Time series of evaporative heat flux (upper panel), computed from hourly data (solid line) and daily averaged data (dotted line), and their difference (hourly − daily, lower panel).

Table 3. Upper ocean heat transport in the WP.

Reference	Description	D (W m^{-2})
Observational study in the WP (*7*)	$D = D_a + D_e$	5 to 19
Observational study between 150°E and 180°E (*22*)	D_a	0
	D_e	<20
R/V *Franklin* cruise data (*8*) (location: 0° to 5°S; 143°E to 150°E; 10 January to 3 February 1986)	D_e	≈3
	D	<10
Coupled ocean-atmosphere model study (*28*)	D	<20
Primitive equation model of the equatorial ocean (*29*)	D_a	4
	D_e	9
	D	13

110 W m^{-2} with a range of $90 < (E + h) < 125$ W m^{-2}. Recent observational and modeling studies (*7*, *8*, *28*, *29*) imply that dynamical heat transport from the mixed layer, D, is less than 20 W m^{-2} and most likely (*8*, *29*) less than 10 W m^{-2} (Table 3). Although the data suggest a range ($10 \leq D \leq 20$ W m^{-2}), we adopted 20 W m^{-2} as our best estimate (Fig. 1). We also estimated SW cloud forcing at the surface by letting $Q = 0.0$ in Eq. 2, which yields

$$C_s(S) = -(S_a - F - E - h - D) \quad (3)$$

Upon using the central, upper, and lower values of the various quantities (Fig. 1), we obtained a value for $C_s(S)$ of -100 W m^{-2} and a range of $-135 < C_s(S) < -80$ W m^{-2}.

Even though we adopted central values (or our best estimate) for the surface cooling terms and maximum values for F, h, and D, the required magnitude of $C_s(S)$ to close the WP heat budget is still large (≈ -100 W m^{-2}). The only direct observational estimate for C_s is the ERBE 5-year average TOA value, which is -66 W m^{-2}. The error in the ERBE value due to temporal and spatial sampling should be negligible, and the bias error (*30*) is estimated to be less than 10 W m^{-2}.

The large value of $C_s(S)$, when compared with the ERBE $C_s(TOA)$ value, suggests that clouds (or cloudy skies) enhance the atmospheric solar absorption significantly, compared with clear-sky solar absorption. The ratio, $f_s = C_s(S)/C_s(TOA)$, is ≈ 1.5 for our optimum values (Fig. 1). Model results (Fig. 3) (*31*) suggest that irrespective of the value of the optical depth or the cloud phase (water or ice cloud) or the height of clouds, $f_s < 1.2$. With a few exceptions (*32*), current radiation models suggest that clouds act merely to shade the sea surface from solar radiation with very little effect on the vertically integrated atmospheric absorption.

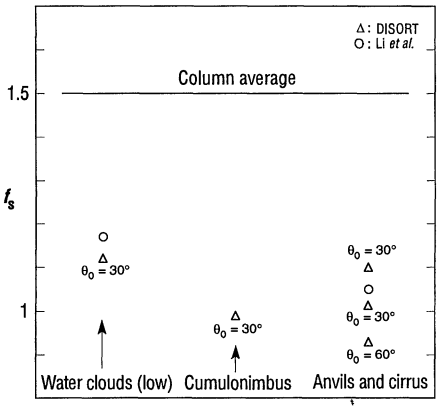

Fig. 3. Comparison of the value for f_s inferred in this study with computed values (*31*) of f_s for different cloud types and for two different radiation models: DISORT and Li *et al.* (*12*). Low clouds in the DISORT code have tops at 3 km and bases at 1 km with an effective radius of 10 μm. The cirrus clouds are 1 km thick with tops at 10 km, and the anvils are 3 km thick with tops at 12 km. The cumulonimbus clouds are 6 km thick with tops at 12 km. The effective particle radius in DISORT is 60 μm for all clouds except low clouds. We use a modified gamma distribution function for equivalent spheres. The spectrum ranges from 0.2 to 4.0 μm; θ_0 is the solar zenith angle. From the Li *et al.* model (*12*), we used ERBE albedos and ship sondes as input.

There are several uncertainties in our approach, which result from uncertainties in the values, particularly those for E and D. In addition, f_s depends on the accuracy of ERBE-derived values for $C_s(TOA)$. If we make the extreme (but plausible) assumption that $C_s(TOA) = -72$ W m^{-2} (a bias error of 6 W m^{-2}) and in addition assume maximum values for F (45), $E + h$ (125), and D (20), the required value for f_s reduces to about 1.2 (= 85/72).

We need collocated observations of TOA and surface solar radiation to verify our inference that $f_s \approx 1.5$. Cess *et al.* (*2*) compared ERBE and GOES observations with simultaneous observations of solar radiation measurements at several surface stations. Their data demonstrate that there was a large and unexplained solar absorption (as much as 25 W m^{-2} globally) in cloudy atmospheres.

Irrespective of the actual value of f_s, our results highlight a fundamental gap in our knowledge. We do not know whether clouds significantly enhance or have no effect on the atmospheric solar absorption. Additional in situ radiometric observations are needed to establish the magnitude of this effect. If the true value for f_s is about 1.5, the atmospheric solar absorption above the WP will increase by about 35 W m^{-2} (from its clear-sky value of 100 W m^{-2}), and the WP mixed layer solar heating will decrease by 35 W m^{-2}. These changes are about 25 to 50% of the excess energy that has to be transported from the equatorial regions to the extra tropics by the atmosphere and the ocean. We conclude that the excess solar absorption in the atmosphere will have an effect on the role of tropical clouds in climate and climate change through their effects on the net equator-to-pole heating gradient of the atmosphere and the oceans, the hydrological cycle, and the surface heat budget (*33*).

REFERENCES AND NOTES

1. E. F. Harrison *et al.*, *J. Geophys. Res.* **95**, 18687 (1990).
2. R. D. Cess *et al.*, *Science* **267**, 496 (1995).
3. C. Zhang, *J. Climate* **6**, 1898 (1993).
4. J. T. Crowley, *Bull. Am. Meteorol. Soc.* **74**, 122363 (1993).
5. The supplement of *J. Geophys. Res.* **96** (28 February 1991) is dedicated to the TOGA program.
6. TOGA-COARE (*5*) stands for Tropical Ocean Global Atmosphere–Coupled Ocean Atmosphere Response Experiment, and CEPEX stands for Central Equatorial Pacific Experiment. These two field experiments were conducted from November 1992 to February 1993 and March to April 1993, respectively. CEPEX is documented in the CEPEX Experiment Design Document (available from the Scripps Institution of Oceanography, University of California, San Diego).
7. P. Niiler and J. Stevenson, *J. Mar. Res.* **40**, 465 (1982).
8. J. S. Godfrey and E. J. Lindstrom, *J. Geophys. Res.* **94**, 8007 (1989).
9. The heat storage in the mixed layer should be 0 for annual mean conditions. Because of interannual variability, Q may not be 0 for any one year, but averaged over several years, $Q \approx 0$.
10. Abbreviations are as follows: COADS, Comprehensive Ocean-Atmosphere Data Set [S. D. Woodruff, R. J. Slutz, R. L. Jenne, P. M. Steurer, *Bull. Am. Meteorol. Soc.* **68**, 1239, (1987)]; ERBE, Earth Radiation Budget Experiment [B. R. Barkstrom *et al.*, *ibid.* **70**, 1254 (1989)]; and TOGA-TAO, TOGA Tropical Atmosphere Ocean Array [M. J. McPhaden, *Oceanography* **6**, 36 (1993)].
11. J. T. Kiehl, J. J. Hack, B. P. Briegleb, *J. Geophys. Res.*. **99**, 20815 (1994). This study uses the CCM2 version of the community climate model. The interannual standard deviations, 1σ, of the yearly means of the various quantities are (in W m^{-2}): $S_a \leq 0.1$; $C_s(TOA) \approx 5$; $C_s(S) \approx 5$; $F_a \leq 0.5$; and $C_l(S) \leq 2$. The interannual standard deviations, 1σ, of the monthly means of the various quantities are (in W m^{-2}): $S_a \leq 1$; $C_s(TOA) \approx 15$; $C_s(S) \approx 15$; $F_a \leq 4$; and $C_l(S) \leq 5$.
12. Z. Q. Li, H. G. Leighton, K. Masuda, T. Takashima, *J. Climate* **6**, 317 (1993).
13. Li *et al.*'s transfer function (*12*) is a function of TOA clear-sky albedo, solar zenith angle, and column water vapor amount and has been validated for clear skies with surface observations [Z. Q. Li, H. G. Leighton, R. D. Cess, *J. Climate* **6**, 1794 (1993)]. The surface fluxes were computed on a monthly basis. We used monthly mean values of A from ERBE; for the column water vapor, we used humidity profiles (96 in all) taken from ships over the WP, during 1985 to 1990, which include a mixture of clear and cloudy conditions. The column water vapor varies between 47 to 55 kg m^{-2}. Li *et al.* used midlatitude ozone amounts. We accounted for the smaller amount of equatorial ozone by adding about 1.5 W m^{-2} to surface insolation.
14. We obtained the solar fluxes by a pyranometer mounted on the R/V *Vickers*. Data were collected once every minute during its cruise along the 2°S latitude line between 168°E and 158°W. Clear-sky downward solar fluxes as a function of solar zenith angle were estimated as follows. Visual report of clear-sky conditions was used to screen the data; next, the flux value that had a maximum number density of points was adopted as the clear-sky value. The downward solar flux was multiplied by $(1 - a_c)$, where a_c is the zenith angle–dependent ocean surface albedo previously described [B. Briegleb and V. Ramanathan, *J. Appl. Meteorol.* **21**, 1160 (1982)].
15. Clear-sky scenes were identified for 1985 by collocation of ERBE clear-sky data with the pyranometer data from American Samoa described in Cess *et al.* (*2*). The downward solar flux was multiplied by $(1 - a_c)$ as in (*14*).
16. Furthermore, because the monthly and annual values for 1σ are only (*11*) 1 and 0.1 W m^{-2}, sampling error was also not an issue. The range of 10 W m^{-2} results from the instrumental uncertainty of about 3%.
17. The radiation model used here is the same as that described [A. Inamdar and V. Ramanathan, *J. Climate* **7**, 715 (1994)], with one exception: We used the LOWTRAN7 version [F. X. Kneizys *et al.*, *Technical Report AFGL-TR-88-0177* (Air Force Geophysics Laboratory, Hanscomb Air Force Base, MA, 1988)].
18. The standard deviation, 1σ, of F_a from the individual sounding was 8 W m^{-2}. Assuming independence between the 96 soundings, the sampling error was ≈ 8 W $m^{-2}/\sqrt{96} \approx 1$ W m^{-2}.
19. The vertical distribution of clouds was taken from ISCCP [W. B. Rossow and R. A. Schiffer, *Bull. Am. Meteorol. Soc.* **72**, 12 (1991)] for middle and high

clouds and from S. G. Warren *et al.* [*Technical Report DOE/ER 0406, NCAR/TN-17+SRT* (NCAR, Boulder, CO, December 1988] for low and cumulonimbus clouds. All clouds were assumed to be black. Cloud-base altitudes for low and cumulonimbus clouds were taken from Warren *et al.*'s atlas. We use ERBE outgoing LW radiation data as a constraint for adjusting the high cloud-top altitudes. We adjusted the ISCCP cloud-top altitudes for cirrus clouds until the computed TOA outgoing long-wave radiation for cloudy skies agreed with ERBE values within a few watts per square meter. This procedure amounted to increasing cirrus altitudes by about 4 km. The cloud thickness was assumed to be 1.5 km, except for cumulonimbus, where the cloud top was taken at 16-km altitude.

20. In this method, the computed values for $C_l(S)$ and $C_l(TOA)$ were used to estimate the ratio f_l, where $f_l = C_l(S)/C_l(TOA)$. The mean value of f_l for the WP region is about 0.3. The ratio increases from about 0.1 to 0.2 for cirrus clouds to about 0.9 for low clouds, yielding a mean value of 0.3. From ERBE data, the 5-year mean LW cloud forcing for the WP at TOA is 62 W m^{-2}. We estimated the 5-year annual mean $C_l(S)$ by letting $C_l(S) = f_l \times C_l(TOA) = 0.3 \times 62 \approx 19$ W m^{-2}.
21. TOGA-COARE cruise data were taken by an upward-looking calibrated pyrometer onboard the R/V *Vickers* from 2 February to 28 February 1994 in the WP at 156°E and the equator. The data and the techniques are as described [L. Schanz, thesis, Universität Hamburg, Germany (1994)].
22. G. S. Young, D. V. Ledvina, C. W. Fairall, *J. Geophys. Res.* **97**, 9595 (1992).
23. S. K. Esbensen and Y. Kushnir, *Technical Report 29* (Climate Research Institute, Oregon State University, Corvallis, 1981).
24. G. J. Zhang and M. J. McPhaden, *J. Climate*, in press.
25. The hourly data used for this comparison were collected from buoys located at 156°E and the equator; 156°E and 2°S; and 165°E and the equator. The time period covered by the hourly data is approximately from September 1992 to March 1993, including the TOGA-COARE period. The hourly fluxes were obtained by direct application of the bulk aerodynamic formulas to the hourly data. We obtained the fluxes from the daily averaged data by first averaging the hourly data to produce daily data and then applying the bulk aerodynamic formulas to the daily averaged data.
26. J. M. Oberhuber, *Technical Report 15* (Max-Planck-Institute for Meteorology, Hamburg, FRG, 1988).
27. R. T. Gosnell, C. W. Fairall, P. T. Webster, *Eos* **74: 43**, 125 (fall meeting suppl. 1993).
28. C. Gordon, *Philos. Trans. R. Soc. London Ser. A* **329**, 207 (1989).
29. P. R. Gent, *J. Geophys. Res.* **96**, 3323 (1991).
30. The spatial and temporal sampling errors should be within a few watts per square meter because of the massive amount of data values (at least 300,000 values) that had gone into the average. However, there may be potential errors, as large as 5 to 10 W m^{-2}, because of the algorithms used to convert satellite radiances to fluxes (J. A. Coakley, personal communication).
31. The model results shown in Fig. 3 use two independent radiation models. (i) DISORT is a comprehensive and computationally accurate multiple scattering code for the solar spectrum. This model is described in K. Stamnes *et al.*, *J. Atmos. Sci.* **38**, 387 (1988). (ii) Li *et al.* results shown in Fig. 3 use the model and algorithms described in Li *et al.* (*12*).
32. W. J. Wiscombe, R. M. Welch, W. D. Hall, *J. Atmos. Sci.* **41**, 1336 (1984); W. J. Wiscombe, *ibid.* **43**, 401 (1986). These papers suggest that the presence of large drops (radius > 100 μm) can enhance atmospheric absorption significantly. A thorough discussion of the controversies surrounding the so-called anomalous cloud absorption can be found in G. L. Stephens and S.-C. Tsay [*Q. J. R. Meteorol. Soc.* **116**, 671 (1990)].
33. J. T. Kiehl, *Phys. Today* **47**, 36 (November 1994).

24 August 1994; accepted 14 November 1994

Clustering and Periodic Recurrence of Microearthquakes on the San Andreas Fault at Parkfield, California

R. M. Nadeau, W. Foxall, T. V. McEvilly

The San Andreas fault at Parkfield, California, apparently late in an interval between repeating magnitude 6 earthquakes, is yielding to tectonic loading partly by seismic slip concentrated in a relatively sparse distribution of small clusters (<20-meter radius) of microearthquakes. Within these clusters, which account for 63% of the earthquakes in a 1987–92 study interval, virtually identical small earthquakes occurred with a regularity that can be described by the statistical model used previously in forecasting large characteristic earthquakes. Sympathetic occurrence of microearthquakes in nearby clusters was observed within a range of about 200 meters at communication speeds of 10 to 100 centimeters per second. The rate of earthquake occurrence, particularly at depth, increased significantly during the study period, but the fraction of earthquakes that were cluster members decreased.

Conceptual methods for earthquake forecasting and hazard mitigation depend critically on the process of fault slip being time-varying in a predictable manner, and evidence for such behavior has been elusive (*1*). In this report we describe patterns of microseismicity that show clustering in space, periodic recurrence, and systematic changes with time on the Parkfield stretch of the San Andreas fault, and we discuss possible mechanisms for this behavior.

Since 1987, seismicity near Parkfield, California, has been monitored with a network of sensitive seismographs installed in boreholes. This stretch of the San Andreas fault has experienced magnitude (M) 6 earthquakes on average every 22 years, on the basis of the record from 1857 to 1966 (*2*). Hypocenter locations for the last three events in the sequence define a common nucleation zone on the fault to within a few kilometers. A diverse earthquake prediction experiment is underway at Parkfield to establish a baseline of parameters that may reveal anomalous behavior before the next M 6 event (*3*).

Approximately 3000 earthquakes were recorded and located from January 1987 to June 1994 on the central 25-km-long section of the fault zone being studied. A three-dimensional model for *P* and *S* wave velocities for this segment has been developed from the microearthquake data (*4*). The small earthquakes are concentrated along a slipping fault zone that is characterized by locally depressed seismic wave velocities, particularly the shear-wave velocity (V_s), and by a region of elevated V_p/V_s near the presumed nucleation volume of the repeating M 6 earthquakes (V_p, *P* wave velocity).

Earth Sciences Division, Lawrence Berkeley Laboratory, and Seismographic Station, University of California, Berkeley, CA 94720, USA.

More than half of the earthquakes can be grouped spatially into small clusters within which events exhibit highly similar recorded waveforms, in many cases over the full 100-Hz bandwidth of the data (Fig. 1) (*5*). The generation of near-identical waveforms at wavelengths as short as 50 m suggests that the sources of seismic wave radiation for these clustered events are essentially repeating ruptures on a common slip surface. We are dealing mainly with small earthquakes in the magnitude range 0 to 1 on fault surfaces with dimensions of a few meters (*6*). The largest events studied have conventionally estimated source dimensions of a few tens of meters, although it is possible that the source dimension has been overestimated because of attenuation effects (*7*). Within the individual clusters, where relative location resolution is a few meters, we can study fault zone dynamics at a scale approaching that of large laboratory experiments.

To analyze the clustering phenomenon quantitatively, we assigned the ~1700 earthquakes in the 1987–92 period to event clusters using an equivalency class (EC) algorithm (*8*, *9*), and the assignments were further refined by visual inspection and regrouping. The similarity measure, β, used in the EC organization is based on a network-wide characterization of maximum cross-correlation coefficient values for *P* and *S* waves between pairs of earthquakes, and it varies systematically with the distance (offset) separating event pairs (Fig. 2). An unexpected result of this analysis was that the correlated earthquake pairs tended to fall into two distinct, offset-dependent populations. One group ($\beta > 0.9$) contains event pairs separated by less than about 200 m, and the other group contains those pairs ($\beta < 0.6$) having offsets greater than 500 m. The β versus offset relation seen for the